Journal of Materials Chemistry B

RSC Publishing

PAPER

Core–shell designs of photoluminescent nanodiamonds with porous silica coatings for bioimaging and drug delivery I: fabrication†

Cite this: J. Mater. Chem. B, 2013, 1, 2358

Eva von Haartman,[a] Hua Jiang,[b] Andrei A. Khomich,[c] Jixi Zhang,[ad] Sergey A. Burikov,[e] Tatiana A. Dolenko,[e] Janne Ruokolainen,[b] Hongchen Gu,[d] Olga A. Shenderova,[f] Igor I. Vlasov*[c] and Jessica M. Rosenholm*[a]

A multifunctional core–shell nanocomposite platform consisting of a photoluminescent nanodiamond (ND) core with uniform porous silica coatings is presented. This design intended for drug delivery applications allows simultaneous stable fluorescent imaging with high loading capacity of bioactive molecules. Despite irregularly shaped starting cores, well-dispersed and uniformly shaped nanocomposite particles can be produced. Moreover, after optimization of the silica source-to-diamond ratio, the thickness of the porous layer can be tuned by adjusting the ethanol amount, allowing rational nanoparticle size control. The ND key property, photoluminescence, is not quenched regardless of coating with thick silica layers. The high loading capacity for incorporation of active agents, provided by the introduced porous layer, is demonstrated by adsorption of a hydrophobic model drug to the composite particles. The loading degree, as compared to a pure ND, increased by two orders of magnitude from 1 wt% for the ND to >100 wt% for the composite particles. Combining these two material classes, which both have well-documented excellent performance especially in biomedical applications, for the NDs with emphasis, but not exclusively, on imaging and mesoporous silica (MSN) on drug delivery, the advantages of both are shown here to be synergistically integrated into one multifunctional nanocomposite platform.

Received 5th March 2013
Accepted 12th March 2013

DOI: 10.1039/c3tb20308e

www.rsc.org/MaterialsB

1 Introduction

In the current race for the improvement of nanotechnology, nanodiamonds (NDs) have recently taken the stage as a promising candidate for a range of nanotechnology-based applications, especially within the biomedical field.[1–3] This notation is explained by a range of promising results regarding the use of luminescent NDs serving as bright, stable imaging probes, applicable for biolabeling.[2–4] NDs have, in these terms, been highlighted over conventional imaging probes such as fluorescent dye molecules due to their problems with photobleaching over time, whereas fluorescent semiconductor nanoparticles (quantum dots) suffer from blinking and toxicity.[5,6] In contrast, NDs have been found to be safe in various biological settings.[1] The development of luminescent NDs has mostly focused on the formation of "nitrogen-vacancy" (NV) color centers in a core of diamond nanoparticles synthesized by the high-pressure high-temperature (HPHT) method.[7] When excited by a laser, the NV centers luminesce in the far-red region that is efficiently capable of penetrating tissue[8] and is well-separated from tissue and cellular autofluorescence. Recently, the presence of NV centers was detected also in ND particles produced by shock-wave assisted methods.[9,10] An additional source of luminescence in diamonds is the structural defects of the diamond surface. The intensity of this type of fluorescence per volume unit increases with decreasing diamond particle size[11] in contrast to the color center fluorescence, which remains unchanged in a volume unit. An additional advantage of the surface fluorescence is the possibility of its essential enhancement by various surface functionalization strategies.[12] Thus, owing to the diversity of the native ND surface heterogeneity, many attempts for the controlled organic modification of NDs

[a]Centre for Functional Materials, Laboratory for Physical Chemistry, Department of Natural Sciences, Åbo Akademi University, 20500 Turku, Finland. E-mail: jerosenh@abo.fi

[b]Nanomicroscopy Centre, Aalto University, FI-00076 AALTO, Espoo, Finland

[c]General Physics Institute, Russian Academy of Sciences, 119991 Moscow, Russia. E-mail: vlasov@nsc.gpi.ru

[d]Nano Biomedical Research Centre, School of Biomedical Engineering and Med-X Research Institute, Shanghai Jiao Tong University, Huashan Rd. 200030, Shanghai, P.R. China

[e]Moscow State University, 119991 Moscow, Russia

[f]International Technology Centre, Raleigh, North Carolina 27617, USA

† Electronic supplementary information (ESI) available: Dynamic light scattering measurements of starting ND cores as well as ND@MSNs; FT-IR spectra of composites before and after extraction of CTAB; photoluminescence stability measurements; powder X-ray diffraction of both ND@MSNs; SEM image and elemental analysis of sample CTAB/TEOS 10/20; nanodiamond/silica ratio calculation procedure. See DOI: 10.1039/c3tb20308e

have been reported.[13–16] The surface fluorescence, however, is furthermore sensitive to the surrounding medium. Thus, a core–shell design comprised of a ND core surrounded by an inorganic shell would be beneficial for the protection of its surface fluorescence, especially when the ND's foreseen application involves an active biological environment.

Core–shell nanoparticle designs have emerged at the frontier between materials chemistry and many other fields, such as electronics, biomedical, pharmaceutical, optics and catalysis.[17] Among the many types of core–shell designs, inorganic/inorganic nanoparticles have been highlighted as the most important, among which silica (SiO_2) has long been considered the foremost coating material[18] and consequently, such structures are currently among the most important and widely studied architectures in colloid science and nanotechnology.[19] This is due to the superior properties of silica related to its excellent physical and chemical properties in combination with synthetic versatility. Due to its chemical inertness, the ceramic layer provided by a silica shell can protect the underlying core from corrosion or degradation induced by damaging environments such as oxygen.[20] At the same time, it can serve as a spacer to separate the core from additional functionalities which may be added to the nanocomposite in the quest to achieve multifunctionality. A typical design of such multifunctional systems is addition of organic dye molecules to a silica shell-covered magnetic nanoparticle, to render the system traceable using both optical and magnetic (MRI) techniques, thereby creating a multimodal imaging probe. Such a structure prevents the direct contact between the magnetic material and dye molecule, which could lead to luminescence quenching.[18] In addition, the silica layer can confer both steric and electrostatic protection on different cores[19] and therefore enhance the colloidal stability of the system. Silica coatings are able to impart water-solubility to hydrophobic magnetic and semiconductor materials and even introduce biocompatibility to the system.[21] Proper dispersability of nanoparticulate systems is furthermore crucial for any further functionalization steps, the modification strategies of which have been studied comprehensively during the last few decades for silica surfaces. A more recent development is the coating of inorganic nanoparticle cores with (meso)porous silica.[22] Pioneered by Hyeon and co-workers in 2006, they deposited a porous silica shell on hydrophobic magnetic nanoparticles through a seeded growth process.[23] Here, the surfactant molecules (most commonly CTAB, cetyltrimethyl ammonium bromide) not only serve as the pore-generating templates as in the pristine mesoporous silica synthesis, but also as a phase-transfer agent for transferring the hydrophobic iron oxide nanocrystals to the aqueous phase where the silica deposition takes place. This approach has been applied to successfully coat inherently hydrophobic nanocrystals (iron oxides and quantum dots) *via* CTAB-transformation to allow for the design of multifunctional nanocomposite nanoparticles aimed for theranostic applications,[24,25] as well as to directly coat CTAB-capped gold[26] and platinum.[27] Such iron oxide–mesoporous silica core–shell constructs have recently been vastly and successfully applied for loading of a wide variety of bioactive molecules, including anticancer drugs as well as genes for the purpose of drug delivery with concurrent imaging capability using MRI.[23,24,28]

In this study, we introduce a novel inorganic/inorganic core–shell system consisting of a hydrophilic ND core and a mesoporous silica shell, denoted ND@MSN, as a novel multifunctional platform with high drug loading capacity and stable luminescence for optical detection. A single-step synthesis approach to directly coat hydrophilic nanodiamond cores with a mesoporous silica layer using CTAB as the porogen is presented. As a luminescent diamond core, a ND produced from a mixture of graphite–hexogen containing NV centers with characteristic spectral features was used. To demonstrate the broad applicability of the developed method to form porous silica shells on different types of luminescent ND particles, another sample, detonation ND (DND), produced from carbon-containing explosives was also used in this study. To show the added value of a porous layer, large amounts (>100 wt% with respect to the total particle mass) of a hydrophobic model drug were loaded into the pores of the composite particle. Remarkably, the same loading procedure employed for the pure ND core, which is the standard procedure used for NDs in drug delivery, resulted in a loading degree of 1 wt%. On the one hand, this demonstrates the feasibility of the produced nanocomposite as a drug delivery carrier,[29] on the other hand it illustrates the possibility of integrating several imaging agents (optically active core material; in the present case ND + active molecular agent of choice; in the present case a fluorescent dye) with different properties to produce multifunctional nanoparticles potentially aimed at improved future disease diagnostics through synergetic multimodal imaging, if desired.[30]

2 Experimental section

2.1 Production of ND cores

ND-1: the nanodiamond material produced by explosion of charges consisting of a graphite and hexogen mixture (graphite + RDX) was purchased from Real-Dzerzinsk, Russia. The ND powder was additionally purified from residual sp^2 carbon in a mixture of nitric–sulfuric acids (1 : 3). The average size of the primary particles determined by Small Angle X-ray Scattering (SAXS) was 34 nm in this material.[10]

ND-2: the raw ND was purchased from Real-Dzerzinsk, Russia. The sample was synthesized by the detonation of a mixture of trinitrotoluene (TNT) and hexogen in a dry cooling medium consisting of gases, the products of the explosion reaction (predominantly CO_2). It was purified from soot using singlet oxygen in NaOH and HNO_3, and additionally treated in NaCl solution. The sample was further fractionated down to 30–50 nm average volumetric particle size. The average size of the primary particles based on SAXS data in this material was 6 nm.[10]

2.2 Coating with porous silica shells

In a typical synthesis, which was also chosen as the optimized coating procedure for part II of this study,[31] 2.5 mg NDs were dispersed in deionized water to a concentration of 1 mg ml^{-1}.

As synthesis solution, a mixture of absolute ethanol/deionized water/ammonium hydroxide solution (33%) in amounts of 2.9 ml/4.3 ml/40 μl was prepared. The diamond dispersion was added dropwise to the synthesis solution under ultrasonication, and was further ultrasonicated for 30 min. A surfactant solution was made by dissolving 40 mg cetyltrimethylammonium bromide (CTAB) in 660 μl deionized H_2O + 300 μl EtOH (abs). The surfactant solution was added dropwise to the synthesis mixture, which was then sonicated for yet another 30 min before addition of 80 μl tetraethoxy orthosilicate (TEOS) as a silica source. The resultant suspension was stirred overnight at RT, after which the particles were separated by centrifugation at 10 000 rpm for 10 min with the aid of acetone. Subsequently, the still surfactant-filled particles were solvent-extracted three times with ammonium nitrate solution (2 g per 100 ml EtOH) in order to remove the CTAB template, washed with ethanol and finally with acetone. The particles were directly redispersed in acetone to a concentration of 1 mg ml^{-1} with respect to the ND mass and stored at +4 °C.

2.3 Control of silica shell thickness

Firstly, the surfactant/silica source (CTAB/TEOS) ratio was varied with respect to the ND mass in order to investigate the effect on the silica layer thickness, as the starting silica amount should have a direct implication on the amount of silica formed. Secondly, the water/ethanol (H_2O/EtOH) ratio of the suspension was altered to tune the size of the particles, as increasing the water/ethanol ratio could be, based on what is known from previous studies on all-silica nanoparticle formation, expected to result in a decrease in all-over particle size, *i.e.* in this case possibly the silica shell thickness, if similar mechanisms are operative.

2.4 Dissolution of the silica shell for the determination of the SiO_2–ND ratio

10 μl of sample solution (1 mg ND per ml) was diluted in 1 ml of 1 M NaOH solution. The sample was stirred for 24 h at RT. 1 ml of 1 M HCl was added and thoroughly mixed to neutralize the solution. The sample was diluted with Milli-Q water to 20 ml and the pH was adjusted to 1.4 with 1 M HCl. 2 ml of ammonium molybdate solution, 2 ml of tartaric acid solution and 2 ml of reduction solution were added to the samples and Milli-Q water was added until a total sample volume of 50 ml was reached. The sample was mixed thoroughly and the coloured (blue) silicomolybdate complex was allowed to form during 1 hour, after which the absorbance was measured at $\lambda = 815$ nm with a Thermo Scientific Nanodrop 2000c dual-mode UV-Vis spectrophotometer. The SiO_2 concentration of the sample was calculated based on an absorbance standard curve for SiO_2.

2.5 Determination of maximum loading capacity

A 1 mg ml^{-1} solution of DiI (1,1′-dioctadecyl-3,3,3′,3′-tetramethylindocarbocyanine perchlorate) in cyclohexane (CH) was added to a known amount of sample also dispersed in CH, starting with 10 wt%. The sample was sonicated and vortexed for ~2 min. Complete adsorption of the dye was visually observed. The procedure was repeated as long as complete loading could be observed. When the supernatant was not clear of dye anymore, the sample was separated by centrifugation, washed with cyclohexane and vacuum dried. The supernatant was collected for analysis. The same procedure was repeated for the corresponding pure ND with the same amount of DiI. The dye amount in the supernatant was determined by absorbance measurement at 560 nm. The absorbance value was converted to a concentration value based on a standard curve for DiI in cyclohexane. The DiI concentration of the sample was determined by subtracting the concentration of the supernatant from the total concentration of DiI added to the sample. As a double check, the vacuum dried, dye-loaded particles were further weighed, eluted in a known amount of methanol (which is a good solvent for the dye), after which the particles were separated by centrifugation. The elution supernatant was collected and the amount of DiI was determined spectrophotometrically to determine the final "actual" loading degree.

2.6 Characterization methods

Dynamic Light Scattering (DLS) and zeta potential measurements were performed on a Malvern Zetasizer instrument (Model Nano ZS, Malvern, Worcestershire, UK) using the Non-Invasive Back-Scatter (NIBS) technique. The instrument was equipped with a monochromatic red laser beam operating at 632.8 nm. The data were analyzed with the Malvern Dispersion Technology Software version 6.20. *z*-average values are given as DLS size unless otherwise stated. Powder-XRD was recorded using a Kratky compact small-angle system (M. Braun) directly on the particle suspension mounted in a glass capillary. The system is equipped with a position-sensitive detector consisting of 1024 channels of 55.5 μm width each. A Seifert ID-300 X-ray generator, operating at a maximum intensity of 50 kV and 40 mA, provided the Cu K_a radiation at $\lambda = 1.542$ Å. A Ni filter was used to remove K_b radiation and a W filter protected the detector from the primary beam. The sample-to-detector distance was 277 mm. The sample holder was kept under vacuum during the measurements. SEM measurements were performed with a LEO Gemini 1530 scanning electron microscope (LEO, Oberkochen, Germany) with a Thermo Scientific UltraDry Silicon Drift Detector (SDD). The SEM was equipped with SE (secondary electron) and BSE (backscattered electron) detectors as well as an In-Lens detector. The magnification of the obtained image corresponds to a Polaroid 545 print with an image size of 8.9 × 11.4 cm. The aperture was kept at vacuum during analysis. The samples were dropped as acetone suspensions onto double sided copper tape, left to dry, after which they were sputtered with carbon and mounted onto a sample holder. Photoluminescence (PL) spectra were recorded with a LABRAM HR800 spectrometer at room temperature. The PL was excited in the samples by Argon + laser light at 488 nm wavelength. For the PL study, thin layers of ND and ND–silica particles were formed on the surface of Si substrates by drying the particles from acetone suspensions. The laser beam of ~0.1 mW power was focused into 2 μm spots on the layers. The photostability of the ND luminescence was studied under

irradiation of the ND–water suspension with 488 nm Ar laser light of 10 W cm^{-2} power density. The PL was detected with a monochromator (Acton) and PMT detector as described elsewhere.[32] Transmission electron microscopy (TEM) measurement was carried out with a JEOL 2200FS double aberration corrected FEG microscope, operating at 200 kV. TEM samples were prepared by casting a drop of the nanoparticle suspension onto copper grids covered with holey carbon films.

3 Results and discussion

3.1 Nanodiamond core materials

Two water-dispersible ND samples of different production origin, ND-1 and ND-2, were chosen for porous silica coating evaluation. Due to the acidic purification process of these detonation nanodiamonds, the surface charge was rendered negative as a result of oxidized surface groups such as carboxylic acids. The surface charges and other characteristics of the DNDs have been summarized in Table 1.

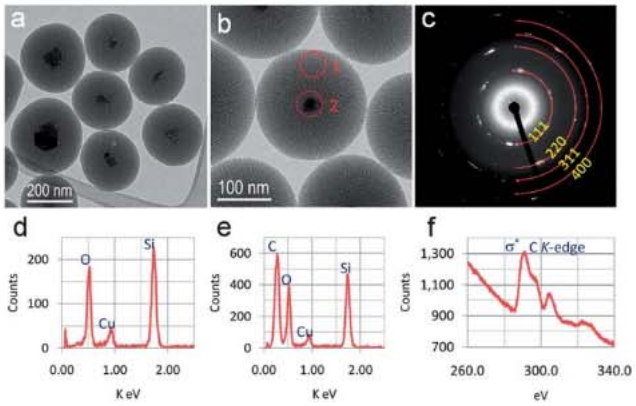

Fig. 1 Transmission electron microscopy studies of the sample ND-1. (a) A typical bright- eld TEM micrograph; (b) a close view of an enlarged nanoparticle in the image center; (c) a selected area electron di raction pattern, indexed for the diamond structure; (d and e) X-ray energy dispersive spectra (EDS) collected from spot 1 and spot 2 in (b), respectively; and (f) C K-edge energy electron energy-loss spectrum (EELS) taken at spot 2 in (b).

3.2 Formation of porous silica shells

Due to the net negative charge of both ND surfaces, we aimed for direct synthesis of mesoporous shells similar to that of what has been used to coat nonporous Stöber silica particles with porous shells.[33] Namely, the synthesis components were the same as those employed for conventional base-catalyzed mesoporous silica (MCM-41) synthesis: water, ammonia, CTAB as a structure-directing agent and TEOS as a silica source with the vital addition of ethanol when corresponding coatings on nanoscaled cores are aimed for.[34,35] For ND-1, which prior to silica coating showed a dynamic light scattering (DLS) *z*-average value centered around 190 nm, shifted to 370 nm after silica coating (ESI, Fig. S1 and S2†). This peak shift along with the low recorded PdI (polydispersity index) value, PdI = 0.067, suggested successful silica coating leading to well-dispersed nanocomposite particles of uniform size. To confirm (1) the successful silica coating along with (2) the formation of a porous structured layer, as well as to determine that (3) the nanocomposite particles actually contained ND cores and no separate all-silica particles had formed, high-resolution transmission electron microscopy was employed (Fig. 1). All material characterizations were performed on surfactant-extracted materials, where the removal of CTAB was confirmed by FTIR (ESI, Fig. S5†).

The morphology and structure of the silica-coated nanodiamond were successfully characterized by TEM. Fig. 1 presents the TEM analysis of sample ND-1@MSN. The bright-field TEM image (Fig. 1a) clearly shows that porous nanocomposite particles had been successfully formed, each containing a single ND core coated with a porous silica layer. An enlarged view of one of the particles is shown in Fig. 1b, where it is seen that the silica pores are radially aligned. Furthermore, the ordered pore structure was also evident from powder X-ray analysis, where one peak at d = 38.5 A was detected (ESI, Fig. S6a†) indicative of typical mesopores of size 3–4 nm.[36] Due to the small domain size and radial alignment from cores of nanoscopic size, no higher order reflection was observed that could be attributed to the typical honeycomb structure of well-ordered bulk MCM-41 type materials.[36] The electron diffraction rings shown in Fig. 1c confirm that the core structure is polycrystalline nanodiamond. Fig. 1d and e show X-ray energy dispersive spectra (EDS) which were collected from spot 1 and spot 2, respectively, indicated by dotted circles in Fig. 1b. Obviously, from the silica layer, only Si and O were detected (Cu signal arises from the copper grid used for supporting samples),

Table 1 Characteristics of the used detonation nanodiamond core materials

Sample notation	Methods of synthesis and treatment of studied samples	Typical size of crystallites[a] [nm]	Used solvents and concentrations in solution	z-potential [mV] @pH 7.2[b] and typical sizes [nm] of ND dispersions[c]
ND-1	Detonation method of synthesis from the mixture of graphite and hexogen, singlet oxygen and acid purification	34	Water, 1 mg ml^{-1}	−23 mV, 200 nm (aq.)
ND-2	Detonation synthesis from the mixture of trinitrotoluene and hexogen, acid purification	6	Water, 1–2 mg ml^{-1}	−36 mV, 120 nm (aq.)

[a] Size was determined by Small Angle X-ray Scattering (SAXS). [b] Zeta potential measurements were performed using HEPES buffer (25 mM, pH 7.2). [c] DLS measurements can be found in the ESI.

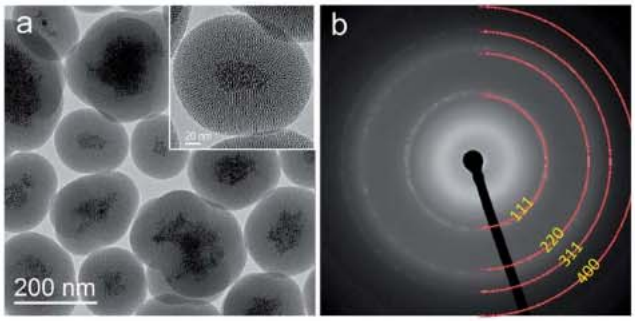

Fig. 2 TEM studies of sample ND-2. (a) A typical bright- eld TEM image (with an enlarged nanoparticle as an inset) and (b) the corresponding electron di raction pattern of the ND-2 porous nanocomposite particles.

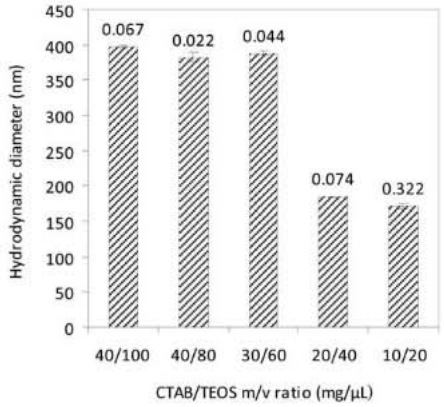

Fig. 3 Variation of DLS size (*z*-average) of the produced ND-1-silica composites with varying CTAB/TEOS amounts. PdI values are given above the columns.

while a strong C signal was observed from the core region in addition to Si and O. In addition, the fine structure of the absorption peak in the electron energy-loss spectrum (EELS) (Fig. 1f) collected in spot 2 contains only a strong π^* peak at about 290 eV, demonstrating the typical carbon K edge for the diamond structure.

To investigate if the same synthesis regime is applicable for multiple ND core types without alteration, we attempted to coat another ND core (ND-2) using the same synthesis. The DLS *z*-average shifted from 80 nm to 260 nm (ESI, Fig. S3 and S4†) and the resultant PdI settled at 0.024. HR-TEM confirmed similar structures as observed for the composites formed from sample ND-2 (Fig. 2).

Similar results were also observed in powder XRD (ESI, Fig. S6b†) as well as TEM for sample ND-2@MSN. Fig. 2 shows (a) a bright-field TEM image with a close-up of one of the nanoparticles in the inset and (b) a selected area electron diffraction pattern. Since the concentration of primary diamond nanoparticles is much higher in ND-2, the electron diffraction pattern shown in Fig. 2b shows more continuous rings which are indexed for the diamond structure. The difference in the ND core structure within the ND core–silica shell structures originates from the difference in the morphologies of the starting DND materials. While ND-1 produced from the mixture of graphite–hexogen are monolithic polycrystalline particles with a minimum size of around 30–40 nm and shapes close to spherical,[10] the ND-2 sample synthesized from a mixture of TNT–RDX consists of 5 nm primary particles connected to porous aggregates of irregular shapes. This distinction is also evident from the DLS results of the initial ND suspensions (ESI, Fig. S1 and S3†) where sample ND-1 resulted in better quality measurement peaks as well as lower PdI than ND-2.

3.2.1 In uence of the CTAB/TEOS-to-ND ratio on the layer thickness. Having established that our applied synthesis regime was suitable for ND coating, we attempted to control the thickness of the porous layer. Firstly, we calculated the approximate yield of the added silica to be less than 60% based on the dry content of the ND–SiO_2 suspensions, and since it was well below 100% yield, we concluded that not all TEOS has been consumed to produce silica shells. Thus, we postulated that we could reduce the TEOS amount and consequently possibly reduce the thickness of the layer when the added silica precursor amount dropped below the 100% yield value. As the TEOS/CTAB ratio is known to be crucial for the formation of MCM-41-type mesophases, this ratio was kept constant but the total amount with respect to the ND and synthesis mixture volume was systematically reduced. As can be seen in Fig. 3, reduction of CTAB/TEOS did not, however, result in any lowering of the hydrodynamic particle size, until a sudden drop to the same DLS size as the pure ND core itself (below CTAB/TEOS ratios of 30 mg / 60 ml).

Elemental analysis (ESI, Fig. S7†) confirmed the presence of carbon only in these samples. Scanning electron microscopy (SEM) analysis also revealed very different structures for the silica-coated samples (Fig. 4b) as compared to ND only suspensions (Fig. 4a). Thus, the silica precursor amount seemed not to be decisive for the thickness of the formed silica layer, as could have been expected from what is known for coating processes of non-porous silica;[37,38] but "any" amount above the critical TEOS/CTAB value would result in the formation of equally thick layers and the rest of the silica would simply not contribute to the shell formation and be discarded in the washing steps.

3.2.2 In uence of the of the H_2O/EtOH ratio on the layer thickness. Given the similarity of the current synthesis composition to that of pristine silica MSN syntheses based on the Stöber process,[39] where co-solvents are pivotal for the formation of uniformly sized spheres, the amount of ethanol was expected to be another crucial parameter for the formed particle morphology. As ethanol is also one of the products formed during the employed sol–gel process, the addition of

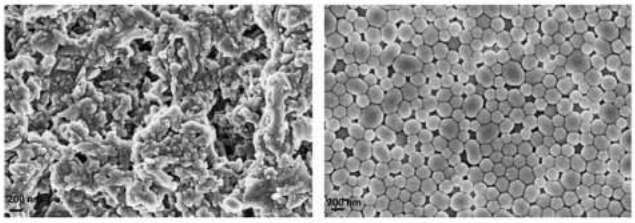

Fig. 4 SEM analysis of the pure ND-1 sample dried from an acetone suspension (left) and of the starting coating-synthesis conditions (CTAB/TEOS 30/60) before the ethanol amount was adjusted (right).

Table 2 The size of the silica-coated ND-1 samples determined by DLS and SEM and the silica coating thickness determined by TEM. Below the blank line the particle SEM size originates from separately formed all-silica particles. All size units are given in nm

Sample	H_2O/EtOH v/v ratio	Size [nm] (DLS)	Size [nm] (SEM)	SiO_2 thickness [nm] (TEM)
1	2.03	393	280	90
2	2.34	375	230	72
3	2.73	335	200	60
4	3.22	311	140	46
5	3.85	285	82	55
6	4.71	271	74	30
7	5.93	265	50	27
8	7.82	254	46	17

ethanol reduces the reaction rate which in turn decreases the local surface curvature energy and leads to the formation of curved morphologies.[40] When the diameter of the core particle decreases, the surface curvature and the corresponding free energy toward shell coating increase dramatically, especially for nano-sized core particles. However, if too much ethanol is added to the reaction medium, the templating ability of CTAB and the aggregation number of surfactant micelles would be disturbed due to the polarity change caused by ethanol. Thus, as the amount of ethanol was not by any means optimized in the above-employed starting synthesis, the ethanol amount was adjusted both upward and downward from this point. Increasing the ethanol amount led to an increase in the recorded DLS size, whereas reduction of ethanol as compared to water slightly decreased the hydrodynamic diameter of the formed composites (Table 2). For detailed structural analysis, HRTEM was also employed in parallel to SEM to study the morphology and architecture of the formed materials (Fig. 5).

When plotted against the adjusted ethanol amount, the particle size follows a decreasing trend with increasing water/ethanol ratio (Fig. 6).

From the SEM images it can be discerned that a systematic diameter decrease for spherical particles takes place (Fig. 5a and c) up to a point where irregular particles start to form (Fig. 5e and g). As can be deduced from the corresponding TEM images, however, this seems to be due to a systematic thinning of the silica layer until the layer is so thin that most of the excess silica precursor forms separate all-silica particles by self-nucleation. The irregularity of the resulting composite particle morphology observed would hence be due to the irregularity of the shape of the ND cores. Remarkably, both the separately formed silica particles as well as the thin silica layers appear to be porous (Fig. 5f and h). The formation of all-silica particles also explains why the mean diameter as approximated from SEM can be smaller than the approximated mean size of ND cores, as the majority of the particles formed at high H_2O/EtOH ratios are very small pure silica particles. For DLS measurements, however, as the employed *z*-average value is based on intensity, large particles are weighed 1 000 000 times with respect to the small particles,[41] and hence the all-silica fraction is largely disregarded and the observed DLS size is actually for

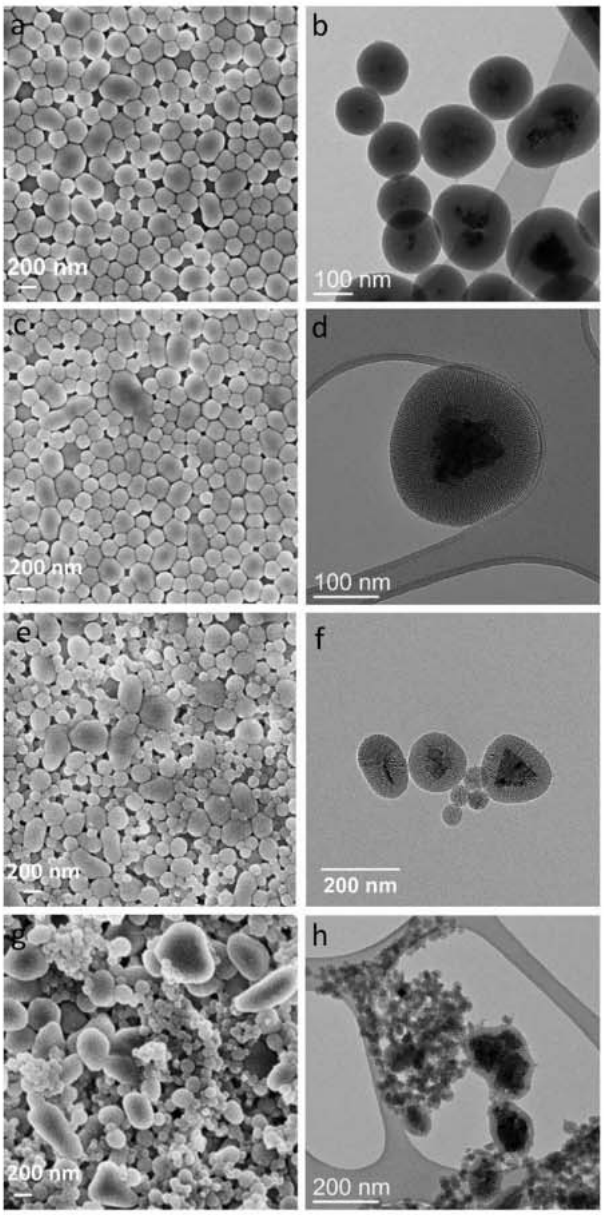

Fig. 5 SEM and corresponding TEM images of selected SiO_2-coated ND-1 samples. The sample names refer to the numbering in Fig. 6 and Table 2 below as follows: (a and b) "2"; (c and d) "3"; (e and f) "5"; (g and h) "8".

the composite particles. The "useful" part of the layer thickness tuning range is thus from the left hand side (up to sample #4) in the graph (Fig. 6) *i.e.* up to a H_2O/EtOH ratio of about 3.2, when the silica layer thickness is about ~46 nm.

3.3 Photoluminescence measurements

To confirm the functionality of the produced nanocomposites, *i.e.* that the silica coating has neither quenched nor decreased the ND photoluminescence (PL), the PL properties of the ND samples were studied before and after their silica coating. The ND-1 sample, produced from the mixture of explosives and graphite, possesses the highest "bulk" (originating from the ND core) luminescence among the main types of detonation diamonds.[10] This "bulk" PL originates from nitrogen-vacancy centers which

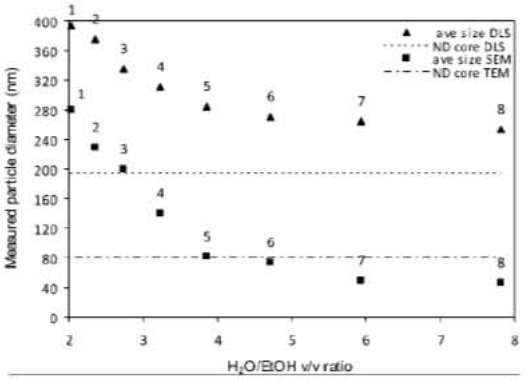

Fig. 6 Particle hydrodynamic size (*z*-average) plotted as a function of the H_2O/EtOH ratio. The size of the silica-coated ND-1 samples as a function of H_2O/EtOH ratio as determined by DLS and SEM (approximate visual determination and calculation from images). The ND core size is also indicated by the straight lines determined by DLS (---) and TEM (---).

are PL active in neutral (NV^0) and negative (NV^-) charge states. Zero-phonon lines (ZPL) of NV^0 and NV^- centers are resolvable at 576 nm and 639 nm, respectively, in the PL spectrum of the ND-1 sample recorded at 488 nm laser excitation (Fig. 7a). The PL spectrum of the ND-2 sample is typical for detonation NDs. It consists of a featureless broad band with a maximum around 600 nm and is reasonably ascribed to surface defects of ND grains (Fig. 7a).[42,43] No "bulk" luminescence was found to be influenced by silica shell covering of the NDs. This is confirmed by the two PL spectra of similar shape and intensity recorded for original ND-1 and for ND-1@MSN with the thickest silica layer (Fig. 7a). In contrast, the "surface" luminescence of ND-2 is increased by about 30% and slightly shifted in position of its maximum (from 610 nm to 580 nm) after silica coating of the sample (Fig. 7b). Thus, the silica layer does not only provide protection of the "surface" luminescence from potential influence of biological environments, but even enhances this luminescence. Notably, the ND-silica particles form more transparent layers than pure ND particles on the Si substrates which were used for PL studies. As a result, a Raman peak originating from the silicon substrate (sharp line near 500 nm) is also detected in the PL spectrum of the ND-1@MSN and ND-2@MSN samples (Fig. 7b and c). The photostability of the ND luminescence was studied for 0.3 mg ml^{-1} water suspensions of ND-1 and ND-2. PL spectra were recorded every 15 min for 2 hour irradiation of the suspensions with 488 nm Ar laser light of 10 W cm^{-2} power density. The integral PL intensity measured in a range of 500–800 nm was slightly decreased (less then 10% of the PL maximum value) for the first 45 min of the measurements and then remained stable with a deviation of 2% relative to the PL mean value for both samples. The dependence of integral PL intensity on time for ND-2 water suspension is shown in the ESI, Fig. S8.† After covering the NDs with silica shells the photostability of the ND luminescence was not altered.

3.4 Hosting of guest molecules

To investigate the potential of the produced porous silica shell for loading of active components, we chose an intensely red

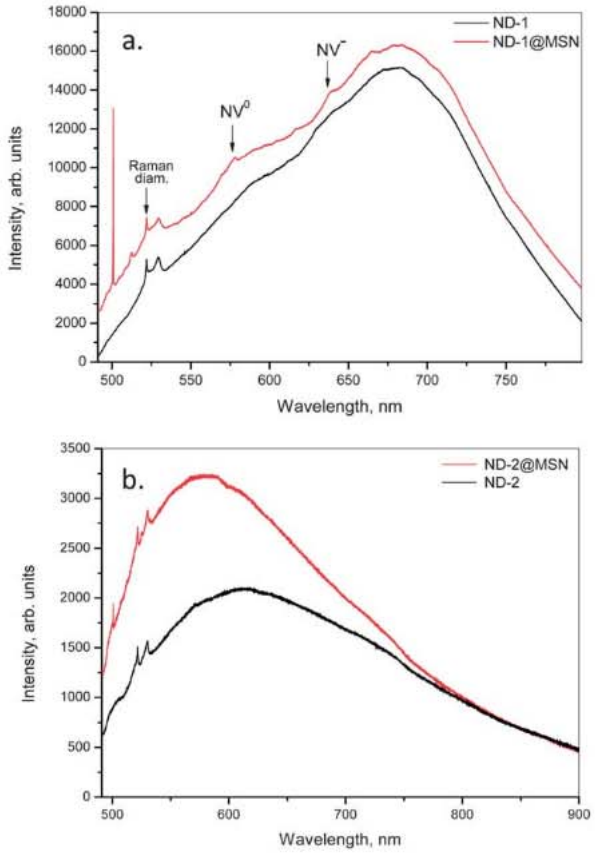

Fig. 7 PL spectra of ND-1 and ND-2 recorded at 488 nm laser excitation at RT. (a) PL spectra of original ND-1 and ND-1 coated with silica (TEOS/CTAB 100/40). The Raman diamond line and ZPLs of NV^0 and NV^- are indicated by arrows at 522 nm, 576 nm, and 639 nm, respectively. (b) PL spectra of original ND-2 and ND-2 coated with silica (TEOS/CTAB 100/40).

hydrophobic dye, DiI, owing to the ease of visualization and thus the possibility for facile real-time titration of the adsorption process (see Fig. 8). Further, using a dye as a model drug compound is facilitative as it can be detected in the visible light range and thus any further modification of the carrier system with organic surface functions will not interfere with its detection, which could be the case if only detectable in the UV range. Even more importantly, owing to its fluorescent properties, the subsequent release under actual biological (*in vitro*) conditions can readily be followed using fluorescence-based techniques such as confocal microscopy, fluorescence-assisted cell sorting and live cell imaging; further allowing the determination of localization, kinetics as well as quantification of delivery efficacy (see Part II). Owing to its hydrophobicity, it simultaneously demonstrates the feasibility of mesoporous silica structures for incorporation of poorly water soluble compounds which is one of the key properties that makes them attractive in biomedical applications.[44] Since approximately 40% of the drugs on the market and about 90% in the development pipeline are poorly soluble in water, rendering formulation essential, the ability to carry hydrophobic cargo is one of the most attractive properties of nanoparticulate formulations. The ND-1@MSN sample with a CTAB/TEOS ratio of 30/60 was chosen for the demonstration.

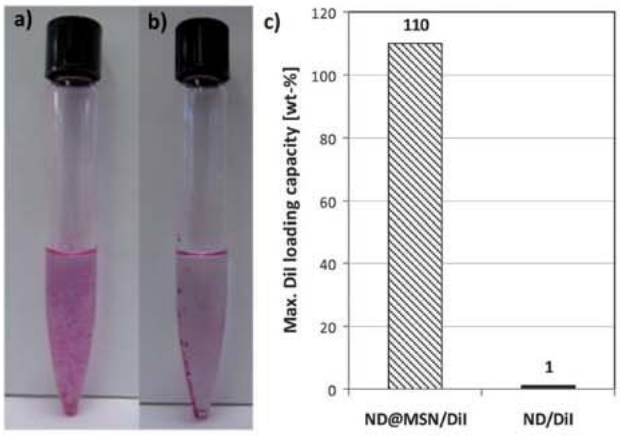

Fig. 8 Loading of active components (uorescent dye DiI) to ND@MSN. Images of the sample (a) before centrifugation where the dye has been adsorbed to the particles and (b) after centrifugation where the supernatant is clear and all dye can be seen adsorbed to the particles. (c) Determination of max. loading capacity in wt% with respect to the total particle mass for pure ND *vs.* ND@MSN.

In order to pinpoint the correct loading capacity, the ND : SiO_2 ratio was first determined using the molybdenum blue method.[45] The ND : SiO_2 mass ratio yielded 1 : 3.15, which is in quite good accordance with theoretical calculations based on approximate sizes of the cores and thickness of the shells (see ESI†). After ND@MSN dispersion into an organic solvent, and subsequent addition of dye solution starting at 10 wt% (with respect to the nanocomposite mass), adsorption could be immediately observed (Fig. 8a). After separation by centrifugation, a red pellet consisting of dye-adsorbed ND@MSNs could be seen while the supernatant was clear of dye (Fig. 8b). Complete adsorption of dye was also confirmed spectrophotometrically. The dye addition was continued until complete adsorption was no longer observed, whereby the particles were separated, washed and vacuum dried. The same procedure was repeated for the pure ND for comparison. For determination of the loading degree, a known mass of dried dye-loaded particles was eluted in methanol, after which the DiI concentration was determined spectrophotometrically. The thus determined loading degree was 110 wt% for the ND@MSN with respect to the total particle mass (DiI/composite). In sharp contrast, employing the same loading procedure to the pure ND core resulted in a loading degree of 1 wt% (Fig. 8c).

Moreover, when the remaining dye in the loading supernatant was analyzed, the obtained loading degrees were 110 wt% for ND@MSN and 19 wt% for the pure ND, indicating that substantial amounts of cargo molecules were lost in the washing step for the pure ND, and thus analyzing only the loading supernatant can lead to large errors if used as the only measure for forthcoming drug delivery evaluations. Further, this illustrates the superior adsorptive properties of the porous silica shell with good affinity towards a range of guest molecules, as the loading degree in the supernatant was the same as in the elution media and thus no cargo was lost in the separation, washing and drying steps, but retained within the carrier. When considering the ND : SiO_2 mass ratio, it could even be postulated that the cargo carrying capacity per ND was increased almost 450× with the addition of the porous silica shell in the case of DiI. We note that the loading degree of specific drug molecules naturally will depend on the molecular characteristics of the compound in question, but the applied loading protocol can readily be utilized as a generic approach for loading of a range of hydrophobic drugs as it relies on increasing the driving force towards adsorption of adsorbates (drugs, in this case) by minimizing the attractive interactions of solvent–adsorbate and solvent–adsorbent under non-polar conditions.[46] Employing the same loading conditions with subsequent elution in methanol to a few example drugs, such as dexamethasone, furesomide and prednisolone, similar loading degrees (up to >100 wt% for drug/composite) could also be obtained. We also note that direct adsorption on the ND surface is the commonly employed loading strategy reported so far for NDs applied for drug delivery purposes,[47,48] and thus our presented design could be considered a significant step forward in ND-based drug delivery systems in terms of loading capacity and carrier uniformity, enabling some interesting advances in the field of inorganic nanomedicine priorly available mainly for magnetic nanoparticles.

4 Conclusions

Successful coating of individual particles of photoluminescent nanodiamonds with mesoporous silica shells has been demonstrated. The coating was obtained in one step and the protocol was reproducible between ND batches of different production origin. The thickness of the resulting porous coatings was shown to be uniform and could furthermore be tuned down to a couple of tens of nanometers. The pores in the coating are radially aligned and feasible for loading of large amounts of active molecules (>100 wt%) as was demonstrated with a hydrophobic model drug molecule. This was in considerable contrast to the adsorption (loading) capacity of the pure ND core, which was 1 wt% in this case. As a key result, even coating with the thickest layers did not quench the luminescence of the ND core, but could, in contrast, provide a protective layer. Given the multifunctional prospects of the developed nanocomposites, biological evaluations to demonstrate the feasibility of the composites as optical probes with in-built drug delivery capacity are presented in part II of this study.[31]

Acknowledgements

All authors want to thank the Academy of Finland and Russian Foundation for Basic Research bilateral project "Fluorescent nanodiamond markers and nanodiamond-silica composites for biology and medicine: Efficiency and stability of photoemission *versus* surface chemistry" (AKA #137101, 10-03-91752-AF_a) for financial support. The authors further acknowledge funding from the Russian Ministry of Education and Science, State contract no. P925 (I.V.), and by the Federal Program of the Russian Ministry of Education and Science, grant 8398 (T.D.), President's grant for leading scientific schools no. 3076.2012.2 (I.V.), and from Russian Academy of Sciences, program no. 24 (I.V.). Finally, Linus Silvander (Abo Akademi University) is acknowledged for SEM imaging.

Notes and references

1 A. M. Schrand, S. A. Ciftan Hens and O. A. Shenderova, *Crit. Rev. Solid State Mater. Sci.*, 2009, **34**, 18.

2 V. N. Mochalin, O. Shenderova, D. Ho and Y. Gogotsi, *Nat. Nanotechnol.*, 2012, **7**, 11.

3 D. Ho, *ACS Nano*, 2009, **3**, 3825.

4 *Nanodiamonds: Applications in Biology and Nanoscale Medicine*, ed. D. Ho, Springer, 2009.

5 V. Biju, T. Itoh, A. Anas, A. Sujith and M. Ishikawa, *Anal. Bioanal. Chem.*, 2008, **391**, 2469.

6 R. Hardman, *Environ. Health Perspect.*, 2006, **114**, 165.

7 J.-P. Boudou, P. A. Curmi, F. Jelezko, J. Wrachtrup, P. Aubert, M. Sennour, G. Balasubramanian, R. Reuter, A. Thorel and E. Gaffet, *Nanotechnology*, 2009, **20**, 235602.

8 F. Neugart, A. Zappe, F. Jelezko, C. Tietz, J. P. Boudou, A. Krueger and J. Wrachtrup, *Nano Lett.*, 2007, **7**, 3588.

9 C. Bradac, T. Gaebel, N. Naidoo, M. J. Sellars, J. Twamley, L. J. Brown, A. S. Barnard, T. Plakhotnik, A. V. Zvyagin and J. R. Rabeau, *Nat. Nanotechnol.*, 2010, **5**, 345.

10 O. A. Shenderova, I. I. Vlasov, S. Turner, G. Van Tendeloo, S. B. Orlinskii, A. A. Shiryaev, A. A. Khomich, S. N. Sulyanov, F. Jelezko and J. Wrachtrup, *J. Phys. Chem. C*, 2011, **115**, 14014.

11 P. H. Chung, E. Perevedentseva and C. L. Cheng, *Surf. Sci.*, 2007, **601**, 3866.

12 V. N. Mochalin, O. Shenderova, D. Ho and Y. Gogotsi, *Nat. Nanotechnol.*, 2011, **201**, 1.

13 H.-F. Wang, Q. Yang and C. Hui Niu, *Diamond Relat. Mater.*, 2010, **19**, 441.

14 T. Burleson, N. Yusuf and A. Stanishevsky, *J. Achiev. Mater. Manuf. Eng.*, 2009, **37**, 258.

15 W.-W. Zheng, Y.-H. Hsieh, Y.-C. Chiu, S.-J. Cai, C.-L. Cheng and C. Chen, *J. Mater. Chem.*, 2009, **19**, 8432.

16 T. Takimoto, T. Chano, S. Shimizu, H. Okabe, M. Ito, M. Morita, T. Kimura, T. Inubushi and N. Komatsu, *Chem. Mater.*, 2010, **22**, 3462.

17 R. G. Chaudhuri and S. Paria, *Chem. Rev.*, 2012, **112**, 2373.

18 W. Schärtl, *Nanoscale*, 2010, **2**, 829.

19 A. Guerrero-Mart nez, J. Perez-Juste and L. Liz-Marzan, *Adv. Mater.*, 2010, **22**, 1182.

20 A.-H. Lu, E. L. Salabas and F. Schüth, *Angew. Chem., Int. Ed.*, 2007, **46**, 1222.

21 S. Simovic, N. Ghouchi-Eskandar, A. M. Sinn, D. Losic and C. A. Prestidge, *Curr. Drug Discovery Technol.*, 2011, **8**, 250.

22 B. Chang, X. Zhang, J. Guo, Y. Sun, H. Tang, Q. Ren and W. Yang, *J. Colloid Interface Sci.*, 2012, **377**, 64.

23 J. Kim, J. E. Lee, J. Lee, J. H. Yu, B. C. Kim, K. An, Y. Hwang, C.-H. Shin, J.-G. Park, J. Kim and T. Hyeon, *J. Am. Chem. Soc.*, 2006, **128**, 688.

24 J. E. Lee, N. Lee, T. Kim, J. Kim and T. Hyeon, *Acc. Chem. Res.*, 2011, **44**, 893.

25 J. Zhang, J. M. Rosenholm and H. Gu, *ChemPhysChem*, 2012, **13**, 2016.

26 I. Gorelikov and N. Matsuura, *Nano Lett.*, 2008, **8**, 369.

27 S. H. Joo, J. Y. Park, C. K. Tsung, Y. Yamada, P. D. Yang and G. A. Somorjai, *Nat. Mater.*, 2009, **8**, 126.

28 X. Li, Q. R. Xie, J. Zhang, W. Xia and H. C. Gu, *Biomaterials*, 2011, **32**, 9546.

29 J. M. Rosenholm, E. Peuhu, J. E. Eriksson, C. Sahlgren and M. Linden, *Nano Lett.*, 2009, **9**, 3308.

30 D.-E. Lee, H. Koo, I.-C. Sun, J. H. Ryu, K. Kim and I. C. Kwon, *Chem. Soc. Rev.*, 2012, **41**, 2656.

31 N. Prabhakar, T. Näreoja, E. von Haartman, D. Şen Karaman, H. Jiang, S. Koho, T. A. Dolenko, P. E. Hänninen, D. I. Vlasov, V. G. Ralchenko, S. Hosomi, I. I. Vlasov, C. Sahlgren and J. M. Rosenholm, *Nanoscale*, DOI: 10.1039/c3nr33926b.

32 T. A. Dolenko, S. A. Burikov, J. M. Rosenholm, O. A. Shenderova and I. I. Vlasov, *J. Phys. Chem. C*, 2012, **116**, 24314.

33 J. H. Kim, S. B. Yoon, J.-Y. Kim, Y. B. Chae and J.-S. Yu, *Colloids Surf., A*, 2008, **313–314**, 77.

34 A. Katiyar, S. Yadav, P. G. Smirniotis and N. G. Pinto, *J. Chromatogr. A*, 2006, **1122**, 13.

35 S. Liu, P. Cool, O. Collart, P. Van Der Voort, E. F. Vansant, O. I. Lebedev, G. Van Tendeloo and M. Jiang, *J. Phys. Chem. B*, 2003, **107**, 10405.

36 C. T. Kresge, M. E. Leonowicz, W. J. Roth and J. C. Vartuli, *Nature*, 1992, **359**, 710.

37 W. Zhao, J. Gu, L. Zhang, H. Chen and J. Shi, *J. Am. Chem. Soc.*, 2005, **127**, 8916.

38 Y. Lu, Y. Yin and Y. Xia, *Nano Lett.*, 2002, **2**, 785.

39 Y. Yamada and K. Yano, *Microporous Mesoporous Mater.*, 2006, **93**, 190.

40 X. Liu, L. Li, Y. Du, Z. Guo, T. T. Ong, Y. Chen, S. C. Ng and Y. Yang, *J. Chromatogr., A*, 2009, **1216**, 7767.

41 Dynamic Light Scattering: An Introduction in 30 minutes. DLS technical note, Malvern Instruments, MRK656-01.

42 P. H. Chung, E. Perevedentseva and C. L. Cheng, *Surf. Sci.*, 2007, **601**, 3866.

43 I. I. Vlasov, O. Shenderova, S. Turner, O. I. Lebedev, A. A. Basov, I. Sildos, M. Rahn, A. A. Shiryaev and G. Van Tendeloo, *Small*, 2010, **6**, 687.

44 J. M. Rosenholm, C. Sahlgren and M. Linden, *Curr. Drug Targets*, 2011, **12**, 1166.

45 C. J. Brinker and G. W. Scherer, *Sol gel Science: The Physics and Chemistry of Sol gel Processing*, Academic Press Inc., 1989.

46 J. M. Rosenholm and M. Linden, *J. Controlled Release*, 2008, **128**, 157.

47 K. Chow, X.-Q. Zhang, M. Chen, R. Lam, E. Robinson, H. Huang, D. Schaffer, E. Osawa, A. Goga and D. Ho, *Sci. Transl. Med.*, 2011, **3**, 73ra21.

48 T. J. Merkel and J. M. DeSimone, *Sci. Transl. Med.*, 2011, **3**, 73ps8.